Simulation of hydrological processes of mountainous watersheds in inland river basins: taking the Heihe Mainstream River as an example

ZhenLiang YIN[1,2], HongLang XIAO[1,2], SongBing ZOU[1,2*], Rui ZHU[3], ZhiXiang LU[1,2], YongChao LAN[1,2], YongPing SHEN[1]

[1] Cold and Arid Regions Environmental and Engineering Research Institute, Chinese Academy of Sciences, Lanzhou 730000, China;
[2] Key Laboratory of Ecohydrology of Inland River Basin, Chinese Academy of Sciences, Lanzhou 730000, China;
[3] College of Earth and Environmental Sciences, Lanzhou University, Lanzhou 730000, China

Abstract: The hydrological processes of mountainous watersheds in inland river basins are complicated. It is absolutely significant to quantify mountainous runoff for social, economic and ecological purposes. This paper takes the mountainous watershed of the Heihe Mainstream River as a study area to simulate the hydrological processes of mountainous watersheds in inland river basins by using the soil and water assessment tool (SWAT) model. SWAT simulation results show that both the Nash–Sutcliffe efficiency and the determination coefficient values of the calibration period (January 1995 to December 2002) and validation period (January 2002 to December 2009) are higher than 0.90, and the percent bias is controlled within ±5%, indicating that the simulation results are satisfactory. According to the SWAT performance, we discussed the yearly and monthly variation trends of the mountainous runoff and the runoff components. The results show that from 1996 to 2009, an indistinctive rising trend was observed for the yearly mountainous runoff, which is mainly recharged by lateral flow, and followed by shallow groundwater runoff and surface runoff. The monthly variation demonstrates that the mountainous runoff decreases slightly from May to July, contrary to other months. The mountainous runoff is mainly recharged by shallow groundwater runoff in January, February, and from October to December, by surface runoff in March and April, and by lateral flow from May to September.

Keywords: hydrological process; mountainous runoff; inland river basin; soil and water assessment tool; the Heihe Mainstream River

Numerous high mountains are located in the upstream areas of inland river basins in Northwestern China. These high mountains become "wet islands" and "water towers" in arid areas because of the intercepted moisture from prevailing air currents. As a result, numerous inland river systems emerged (Cheng and Zhao, 2008). The runoffs generated in the upstream mountainous areas supply the midstream and downstream areas (Ling et al., 2012); thus, the survival and development of the economic and ecological systems of inland river basins are maintained. Therefore, research on hydrological processes in mountainous areas is consistently significant in the resource and environmental fields (Kang et al., 2008). Over the past few decades, researchers have accumulated achievements on the hydrological processes of inland river basins in mountainous areas. Model simulation is considered an effective tool in applying the results of these local

© Xinjiang Institute of Ecology and Geography, Chinese Academy of Sciences, Science Press and Springer-Verlag Berlin Heidelberg 2013

studies in a wider scale (Huang et al., 2012).

The objective of investigating hydrological processes is to provide distributed hydrological models for a specific area by relying on a strict physical basis (Stephen, 1986). The studies on distributed hydrological models in China initiated comparatively late (Rui, 1997). However, in the recent decade, researches on the mountainous watersheds in inland river basins have been developed greatly. For instance, Kang et al. (1999) classified the mountainous watershed of the Heihe Mainstream River into two basic landscape zones, namely, the permafrost-snow-ice zone and the montane vegetation zone, and then established a concept model for the monthly mountainous runoff of the Heihe River by simulating the runoff processes of the mountainous area with the Hydrologiska Byrans Vattenbalans-avdelning (HBV) model. Xia et al. (2003) developed a distributed time variant gain model on the basis of the theory of precipitation-runoff nonlinear system and a conceptive simulation method applied to the upstream of the Heihe River Basin. Huang and Zhang (2004, 2010) divided the mountainous watershed of the Heihe Mainstream River into 157 hydrological response units through the soil and water assessment tool (SWAT) model, and simulated the mountainous runoff. Focusing on the physical mechanism of hydrological cycle in the river basin, Jia et al. (2006) proposed a distributed hydrological model called "water and energy transfer processes (WEP)–Heihe" and applied it to simulate the hydrological processes of the mountainous watershed of the Heihe Mainstream River. Chen et al. (2008) developed a distributed water-heat coupled (DWHC) model for high and cold mountainous areas of inland river basins by considering special hydrological processes. In another study, Li et al. (2011) compared the applicability of two hydrological models with different complexities, namely, water and snow balance modeling system (WASMOD) and SWAT model, by simulating the mountainous runoff in the mountainous watershed of the Heihe Mainstream River. In the above-mentioned studies, researchers have analyzed the hydrological processes in the mountainous areas of inland river basins.

Many existing studies simulated the monthly or daily mountainous runoff in the mountainous watersheds of inland river basins (Kang et al., 1999; Xia et al., 2003; Huang and Zhang, 2004; Jia et al., 2006; Chen et al., 2008; Li et al., 2011); however, few studies discussed the components of mountainous runoff and interannual and annual variations of these components. This article aims to analyze the interannual and annual changes of mountainous runoff components including surface runoff, lateral flow, and shallow groundwater runoff (base flow) by simulating the hydrological processes in the mountainous watershed of the Heihe Mainstream River with the SWAT model.

1 Study area

The mountainous watershed of Heihe Mainstream River (Yingluoxia watershed) is located at the upper reaches of Heihe River Basin. The watershed covers an area of approximately 10,018 km^2, most of which is mountainous. The elevation in the watershed ranges from 1,637 to 5,062 m asl (Fig. 1). The mountainous runoff is monitored by the Yingluoxia hydrological station (38.82°N, 100.18°E; 1,637 m asl) located at the mainstream outlet of the Heihe River flowing from the Qilian Mountains down to the Hexi Corridor Plain. Two hydrological stations, namely Qilian (38.20°N, 100.23°E; 2,590 m asl) and Zhamashike (38.23°N, 99.98°E; 2,635 m asl), are located at the eastern and western tributaries of the Heihe Mainstream River. The climate in the watershed is characterized as cold and dry in winter and hot and humid in summer with large spatial and temporal variabilities. The annual precipitation, which is concentrated mainly in summertime, tends to decrease from east to west and increase along with altitude. Altitudinal landscape zonation exists in the watershed, with desert steppe, dry shrubbery grassland, forest grassland, sub-alpine shrubbery meadow, alpine cold-and-desert meadow, and alpine permafrost-snow-ice ranging from low to high altitudes. The main soil types in the watershed are alpine meadow soil, alpine steppe soil, frigid desert soil, gray cinnamonic soil and gray-brown desert soil.

2 Data and Methodology

2.1 SWAT model

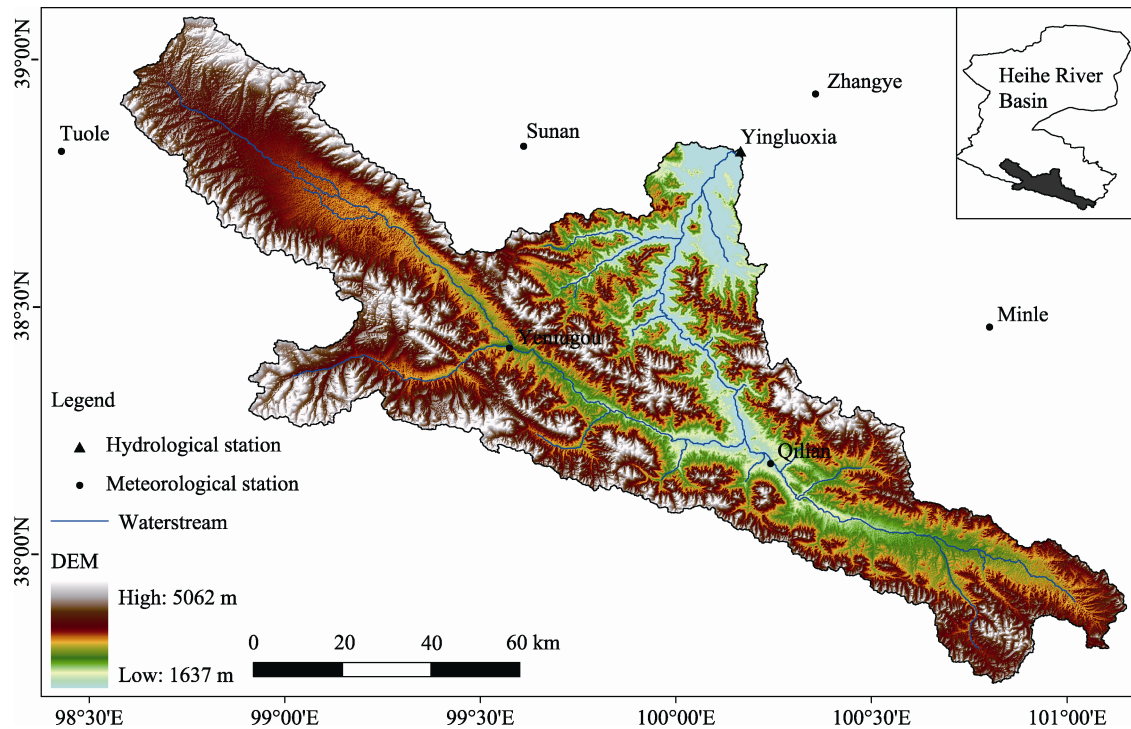SWAT (soil and water assessment tool) model is a

Fig. 1 Location of the mountainous watershed of the Heihe Mainstream River and distribution of hydrological and meteorological stations

physically-based hydrological/water quality model developed by the United States Department of Agriculture (Arnold et al., 1998). The model is a continuous-time, spatially semi-distributed simulator for hydrological cycle and agricultural pollutant transport in a basin scale, and runs on annual, monthly, and daily time steps. Major model components include weather, hydrology, soil temperature and properties, plant nutrients and growth, pesticides, bacteria including pathogens, and land management (Neitsch et al., 2005). In SWAT, a watershed is divided into multiple subwatersheds, which are then further subdivided into hydrologic response units (HRUs) that consist of homogeneous land use and soil types and terrain characteristics. An overall hydrological balance is simulated for each HRU.

The hydrological cycle as simulated by SWAT is based on the following water balance equation:

$$SW_t = SW_0 + \sum_{i=1}^{t}(R_{day} - Q_{surf} - E_a - w_{seep} - Q_{gw}), \quad (1)$$

where SW_t is the final soil water content (mm), SW_0 is the initial soil water content on day i (mm), t is the

time (days), R_{day} is the amount of precipitation on day i (mm), Q_{surf} is the amount of surface runoff on day i (mm), E_a is the amount of ET on day i (mm), w_{seep} is the amount of water entering the vadose zone from the soil profile on day i (mm), and Q_{gw} is the amount of return flow on day i (mm).

The surface runoff is calculated as follows:

$$Q_{surf} = \frac{\left(R_{day} - 0.2S\right)^2}{\left(R_{day} + 0.8S\right)} \quad R_{day} > 0.2S, \quad (2)$$

where Q_{surf} is the amount of surface runoff on day i (mm), R_{day} is the amount of precipitation on day i (mm), and S is the retention parameter (mm), which is calculated as:

$$S = 25.4\left(\frac{1000}{CN} - 10\right), \quad (3)$$

where CN is the curve number for the day.

The lateral flow is calculated as follows:

$$Q_{lat} = 0.024\left(\frac{2 \times SW_{ly,excess} \times K_{sat} \times slp}{\varphi_d \times L_{hill}}\right), \quad (4)$$

where Q_{lat} is the water discharged from the hillslope

outlet (mm/day), $SW_{ly,excess}$ is the drainable water stored in the saturated zone of the hillslope per unit area (mm), K_{sat} is the saturated hydraulic conductivity (mm/h), slp is the increase in elevation per unit distance, φ_d is the drainable porosity of the soil (mm/mm), and L_{hill} is the hillslope length (m).

The shallow groundwater runoff is calculated as follows:

$$Q_{gw} = Q_{gw,i-1} \times \exp\left[-\alpha_{gw} \times \Delta t\right] +$$
$$w_{rchrg,sh} \times \left(1 - \exp\left[-\alpha_{gw} \times \Delta t\right]\right)$$
$$aq_{sh} > aq_{shthr,q}. \tag{5}$$

Where Q_{gw} is the groundwater flow into the main channel on day i (mm), $Q_{gw,i-1}$ is the groundwater flow into the main channel on day i–1 (mm), α_{gw} is the baseflow recession constant, Δt is the time step (1 day), $w_{rchrg,sh}$ is the amount of recharge entering the shallow aquifer on day i (mm), aq_{sh} is the amount of water stored in the shallow aquifer at the beginning of day i (mm) and $aq_{shthr,q}$ is the threshold water level in the shallow aquifer for groundwater contribution to the main channel to occur (mm).

2.2   Data availability

The ASTER GDEM (Global Digital Elevation Map) with a resolution of 30 m was used as the digital elevation model in this study. The hydrological and meteorological observation data, as well as geographic information system referenced soil data and land use map, were all downloaded from the portal of Environmental and Ecological Science Data Center for West China. The soil and land use data were extracted from a 1:1,000,000 soil map and a 1:1,000,000 vegetation map of the Heihe River Basin, respectively. A total of 24 soil types and 14 land use types were available at the study area. Daily data of precipitation, maximum and minimum temperatures, wind speed, and relative humidity were obtained from the records of six meteorological stations (Fig. 1). The solar radiation data were calculated with the Angstrom formula (Allen et al., 1998) by using the observed sunshine hours from the meteorological stations. The monthly hydrological observation data involved in this research were obtained from the observation record of the Yingluoxia hydrological station. We em-

ployed the meteorological and hydrological data from January 1995 to December 2009.

2.3   Model setup

After data preparation, the model setup was prepared by performing the following major steps: (i) watershed delineation and subwatershed characteristics derivation; (ii) hydrological response unit (HRU) definition; (iii) model running and parameter sensitivity analysis; and (iv) model calibration and validation.

During watershed delineation, we divided the study area into 43 subwatersheds, with 10,000 hm^2 as an area threshold. The HRU definition step was performed through the HRU analysis module, which requires data of land use, soil, and watershed slope. HRU refers to an area with unique land use type, soil, and slope combinations. Four classes of slope ranging 0–5$^\mathrm{o}$, 5$^\mathrm{o}$–25$^\mathrm{o}$, 25$^\mathrm{o}$–45$^\mathrm{o}$, and ≥45$^\mathrm{o}$ were addressed.

The model was run by using the prepared meteorological data inputs and HRU information defined in the previous steps. The simulation was run for the calibration period from January 1995 to December 2002 by using the first year as a warm-up period (Fiseha et al., 2012). The model underwent calibration and validation. In SWAT, a large number of parameters used for defining the characteristics of the watershed cannot be accurately characterized by the default input parameters. Therefore, the process of model calibration and validation was executed.

2.4   Statistical evaluation criteria

The quantitative evaluation of each simulation result after parameter adjustment was performed on the basis of the values of some selected descriptive statistics and objective functions to determine the goodness of fit of the selected model. The Nash–Sutcliffe efficiency (NSE) (Nash and Sutcliffe, 1970), the coefficient of determination (R^2) (Legates and McCabe, 1999), and the percent bias (PBIAS) (Gupta et al., 1999) are frequently used in hydrological modeling studies (Krause et al., 2005; Moriasi et al., 2007) and are calculated as follows:

$$NSE = 1 - \frac{\sum_{i=1}^{n}\left(Q_i^{obs} - Q_i^{sim}\right)^2}{\sum_{i=1}^{n}\left(Q_i^{obs} - Q_{avg}^{obs}\right)^2}, \tag{6}$$

$$R^2 = \frac{\left(\sum_{i=1}^{n}(Q_i^{obs} - Q_{avg}^{obs})(Q_i^{sim} - Q_{avg}^{sim})\right)^2}{\sum_{i=1}^{n}\left(Q_i^{obs} - Q_{avg}^{obs}\right)^2 \sum_{i=1}^{n}\left(Q_i^{sim} - Q_{avg}^{sim}\right)^2}, \quad (7)$$

$$PBIAS = \frac{\sum_{i=1}^{n}\left(Q_i^{sim} - Q_i^{obs}\right)}{\sum_{i=1}^{n} Q_i^{obs}} \times 100\%. \quad (8)$$

In which, Q_i^{sim} is the simulated streamflow and Q_i^{obs} is the observed streamflow at time step i, respectively, whereas Q_{avg}^{obs} and Q_{avg}^{sim} are the average observed and simulated streamflow values in time periods 1, 2, …, n.

NSE measures how well model predictions represent the observed data, relative to a prediction made by using the average observed value. NSE ranges from $-\infty$ to 1, with NSE=1 being the optimal value (Nash and Sutcliffe, 1970). R^2 ranges from 0 to 1 and represents the proportion of the total variance in the observed data that can be explained by the model, with higher R^2 values indicating better model performance. PBIAS measures the average tendency of the simulated data, with positive values indicating a model overestimation bias, and negative values indicating a model underestimation bias. The optimal value is 0 (Gupta et al., 1999). Low-magnitude values of PBIAS are preferred.

3   Results and discussion

3.1   Sensitivity analysis and calibration

A sensitivity analysis identifies the most responsive hydrological parameters before calibration by evaluating the change rate in model outputs relative to the model inputs. The Latin Hypercube Sampling One-factor-At-a-Time design method is used to perform the analysis (Morris, 1991). The method employs a modified Monte Carlo simulation that integrates local and global sensitivity of the model parameters (van Griensven et al., 2006).

Table 1 shows the result of the sensitivity analysis on the basis of the 10 most sensitive parameters. The sensitivity analysis result is similar to the result analyzed by Huang and Zhang (2010). The average pre-

cipitation lapse rate, which was set at 159 mm/km for the eastern tributary and 110 mm/km for the western tributary, was computed by analyzing the annual precipitation for 15 years from 1995 to 2009 observed at six meteorological stations. Each subwatershed was divided into three to six elevation bands according to the elevation span of the subwatershed. The elevation at the center of the elevation band and the fraction of subwatershed area within the elevation band were set as well.

### 3.2   Simulation results and applicability assessment

This article chose January 1995 to December 2002 as the calibration period and January 2002 to December 2009 as the validation period. The first years of the two periods were set as warm-up periods. Figure 2 shows the monthly simulated runoff and observed runoff at the Yingluoxia hydrological station. The monthly mean precipitations simulated by SWAT are also demonstrated in Fig. 2. The values of the three selected assessment parameters were calculated. The NSE coefficients were 0.94 and 0.90, the R^2 values were 0.94 and 0.91, and the PBIAS were −2.88% and 4.08% in the two periods, respectively. The NSE and R^2 values were close to 1, and the PBIAS was close to 0, thereby illustrating a satisfactory simulation result.

According to researches summarized by Li et al. (2011), the simulation and assessment results obtained in the present article were prior to the results of previous researches on the runoff simulation in the same area. Most studies on hydrological process simulation in this area simulated temporal interval before 2002 (Kang et al., 1999; Xia et al., 2003; Huang and Zhang, 2004; Jia et al., 2006; Chen et al., 2008). By contrast, the present study extends the simulation period to 2009 to further research the latest variation trends of the mountainous runoff in the mountainous watershed of the Heihe Mainstream River. According to the precision assessment standard (0.75<NSE≤1.00, PBIAS< ±10%) by Moriasi et al. (2007), the simulation results of this study can be labeled as "very good". Therefore, we address that SWAT is capable of effectively and reliably simulating the hydrological processes in the mountainous watershed of the Heihe Mainstream River and can be used to analyze variation of runoff

Table 1 Parameters used for model calibration

Parameter	Description	Range	Initial value	Value chosen	Method	Input file	Level
TLPAS	Temperature lapse rate (°C/km)	−15–15	−6	−5	Replace	.sub	Subwatershed
ALPHA_BF	Baseflow alpha factor (days)	0–1	0.4	*a	Replace	.gw	HRU
SOL_Z	Depth from soil surface to bottom of layer (mm)	0–2,000	Default	1	Multiply by	.sol	HRU
ESCO	Soil evaporation compensation factor	0–1	0.95	0.85	Replace	.bsn	Watershed
CN2	Initial SCS runoff curve number for moisture condition II	50–100	65	−6	Add	.mgt	HRU
CH_K2	Effective hydraulic conductivity in main channel alluvium (mm/hr)	0–50	0	*b	Add	.rte	Subwatershed
SOL_AWC	Available water capacity of the soil layer (mm H_2O/mm soil)	0–1	Default	1	Multiply by	.sol	HRU
CANMX	Maximum canopy storage (mm H_2O)	0–10	Default	1	Multiply by	.hru	HRU
BLAI	Maximum potential leaf area index	0–10	Default	1	Multiply by	Crop.dat	Watershed
SOL_K	Saturated hydraulic conductivity (mm/h)	0–300	Default	1	Multiply by	.sol	HRU

Note: *a, 0.06 in the eastern tributary, 0.072 in the western tributary; and *b, 35 in the eastern tributary, 15 in the western tributary.
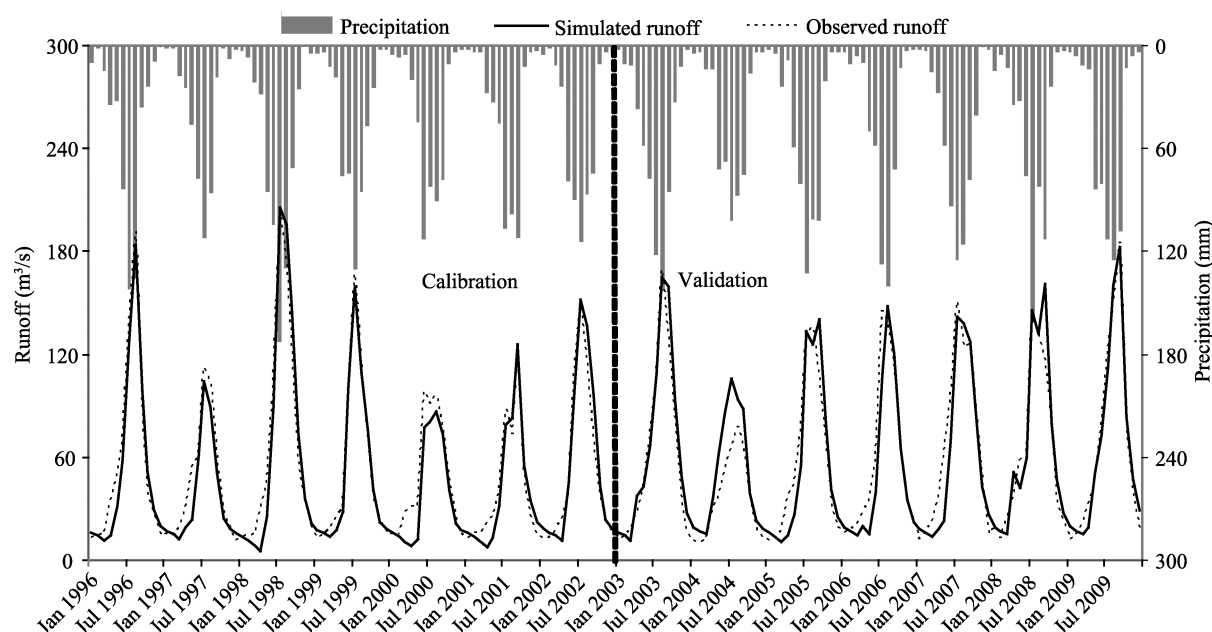
Fig. 2 Calibration and validation results for the monthly runoff at Yingluoxia hydrological station from January 1996 to December 2009

components if no observed data of runoff components are available.

3.3 Interannual variation trends of individual runoff components

The water yield simulated by SWAT consists of three components: surface runoff, lateral flow, and shallow groundwater runoff (base flow). Figure 3 presents the interannual (1996–2009) variation of the simulated mountainous runoff and runoff components. The in-

terannual variation trends of each runoff component are consistent with mountainous runoff variation, and the values for the runoff components generally increase inconspicuously over the recent decades. These results are similar to previous studies (Kang et al., 1999; Lan et al., 1999; Chen et al., 2002), proving that the estimate on the runoff variation trend in this area is correct. Among the three runoff components, the lateral flow contributes most to the mountainous runoff, accounting for 54.5% and exceeding the total contri-

bution of surface runoff and shallow groundwater runoff. The contributions of shallow groundwater runoff and surface runoff to mountainous runoff are 25.2% and 20.3%, respectively.
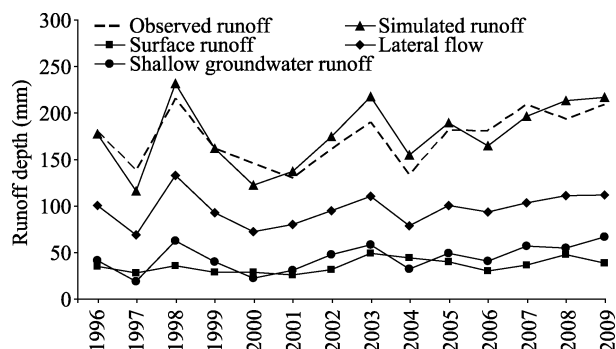

Fig. 3 Interannual variations of individual runoff components from 1996 to 2009

Few studies on the mountainous runoff components of inland rivers are available. Although the isotopic technology enables the separation of runoff into different components (Zhao et al., 2011), the hydrological processes of inland river basins are so complex that the isotopic technology is limited for mountainous runoff separation. For instance, numerous transformations of surface water and groundwater result in their aggregation into a river. The result of this article that the shallow groundwater runoff presents an increasing trend is consistent with the conclusion drawn from the studies on base flow separation in the mountainous watershed of the Heihe Mainstream River (Dang et al., 2011; Zhang et al., 2011). The contribution of shallow groundwater runoff to total runoff is 25.2% in this article, which is slightly different from the 31.0% obtained by Tang et al. (1992) and the 36.7% obtained by Gao and Yang (1984). The difference in partition of groundwater flow in total runoff could be caused by the difference in the choose of the study area. This article focuses only on the mountainous watershed of the Heihe Mainstream River. On the contrary, Tang et al. (1982) and Gao and Yang (1984) calculated the contribution of groundwater flow in the mountainous area of the entire Heihe River Basin.

According to the observations of three typical alpine meadow runoff fields in the mountainous area of the Heihe Mainstream River by Chen et al. (2007), the alpine meadow vegetation buffered and decreased the

rainfall energy to the ground surface. For instance, the thick vegetation and multilayer structure prevented rainfall from generating surface runoff, causing the rainfall to infiltrate slowly into the underground soil through vegetation. This phenomenon partly explains the mechanism in this study that lateral flow provides the greatest contribution to the total mountainous runoff, and surface runoff provides the least contribution.

3.4 Monthly variation trend of individual runoff components

3.4.1 Multi-year monthly mean variations of individual runoff components

We calculated the monthly mean runoff from 1996 to 2009 for each component (Fig. 4). Lateral flow and mountainous runoff have similar variation process in which they peaked in July, maintained high levels from July to September, and sharply declined in October. After October, when the weather became cold and rainfall infrequent, mountainous runoff was generated minimally.
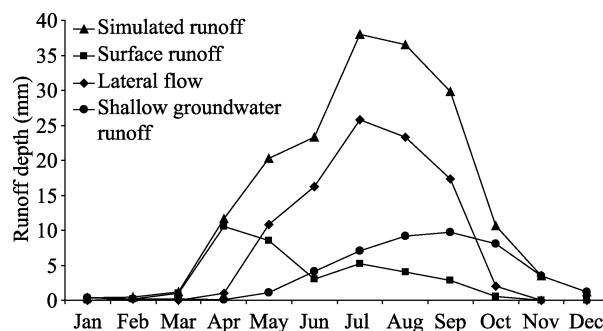

Fig. 4 Multi-year monthly mean variations of individual runoff components

Contrary to lateral flow, surface runoff shows a different annual change process, and reaches its peak in April because of the melting of accumulated snow caused by increasing temperature (Wang and Li, 2006). However, the temperature increase is not enough to melt the permafrost that prevents melted snow from infiltrating into the soil (Jin et al., 2011). Therefore, surface runoff becomes the dominant component in the river from March to April. After April, almost all of the accumulated snow melts completely, precipitation increases, and most of the rainfall infiltrates into the soil, recharging the river in the form of lateral flow (Chen et al., 2007). This occurrence explains the rela-

tive low value of surface runoff in June. Following the maximum precipitation in July, a portion of rainfall flows into the river in the form of surface runoff, resulting in a second peak. The surface flow reduces subsequently as the precipitation decreases in August and continues to decrease in the next four months.

The annual variation of shallow groundwater runoff is relatively simple. Shallow groundwater runoff increases with temperature and precipitation and is at its maximum in September, and then decreases gradually afterward. The shallow groundwater runoff achieves its maximum two months after the mountainous runoff reaches its maximum, thus indicating that the groundwater regulates mountainous runoff.

3.4.2   Monthly variation of runoff components

We also analyzed the variation trends of mountainous runoff and individual runoff components in each month from 1996 to 2009 based on the SWAT performance (Fig. 5).

The mountainous runoff in January and February increases slightly except in 2000 and 2001. The mountainous runoff in January and February is primarily recharged by shallow groundwater, accounting for 99.6% in January and 95.2% in February. In March, as the temperature rises, shallow groundwater runoff is no longer the main runoff component, accounting for only 4.7%. By contrast, the contribution of surface runoff to the mountainous runoff reaches 95.2%. As temperature continues to increase in April, most of the accumulated snow melts, which makes surface runoff become the main runoff component. The surface soil of permafrost begins to melt, resulting in increased lateral flow. Surface runoff accounts for 90.5% of the annual mountainous runoff, lateral flow for 8.3%, and shallow groundwater runoff for only 1.2%.

In contrast with the mountainous runoff from January to April, the mountainous runoff decreases slightly in May. As the temperature continues to increase, the frozen soil melts, precipitation begins to increase, and most of the rainwater infiltrates into the soil. Lateral flow becomes the main runoff component, accounting for 53.0%, surface runoff for 41.7%, and shallow groundwater runoff for 5.3%. The mountainous runoff in June and July also declines slightly. The contribu-

tion of lateral flow to the mountainous runoff continues to increase, reaching 69.5% and 67.7% in June and July, respectively. The shallow groundwater runoff begins to increase as precipitation increases, accounting for 17.7% in June and 18.5% in July, and surface runoff for 12.8% in June and 13.8% in July.

Lateral flow remains as the dominant runoff component, accounting for 63.8% and 57.9% of the mountainous runoff in August and September, respectively. Shallow groundwater runoff accounts for 25.2% in August and 32.6% in September, and surface runoff for 11.0% in August and 9.5% in September. Temperature and precipitation decreases and soil begins to freeze in October, thus rapidly diminishing the lateral flow. Therefore, shallow groundwater runoff becomes the main runoff component. Shallow groundwater runoff accounts for 75.6%, lateral flow for 19.4%, and surface runoff for only 5.0% of the mountainous runoff in October. Shallow groundwater runoff accounts for 99.4% and 99.7% of the mountainous runoff in November and December, respectively.

Previous research on snowmelt runoff in spring suggested that approximately 75% of the mountainous runoff in spring is from snowmelt water (Wang and Li, 2006). The simulation result of this study also shows that the surface runoff is relatively high from March to May. Previous studies on permafrost hydrological processes and freezing and thawing rules showed that the permafrost in the study area begins to melt by the end of April and freeze in the last 10 days of October (Chen et al., 2007; Jin et al., 2011). This finding is consistent with the analyses of this study, which shows that lateral flow begins to increase in April and decreases rapidly in October. Kang et al. (1999) indicated that along with climate changes, the annual increase in mountainous runoff is minimum in inland river basins although it increases in spring and decreases in summer, which is in accordance with the result of this study that mountainous runoff decreases slightly from May to July.

In summary, the multi-year variation trend of the mountainous runoff and the values of the monthly runoff components in the study area decrease slightly from May to July, but generally increase for the entire year. Moreover, mountainous runoff is recharged
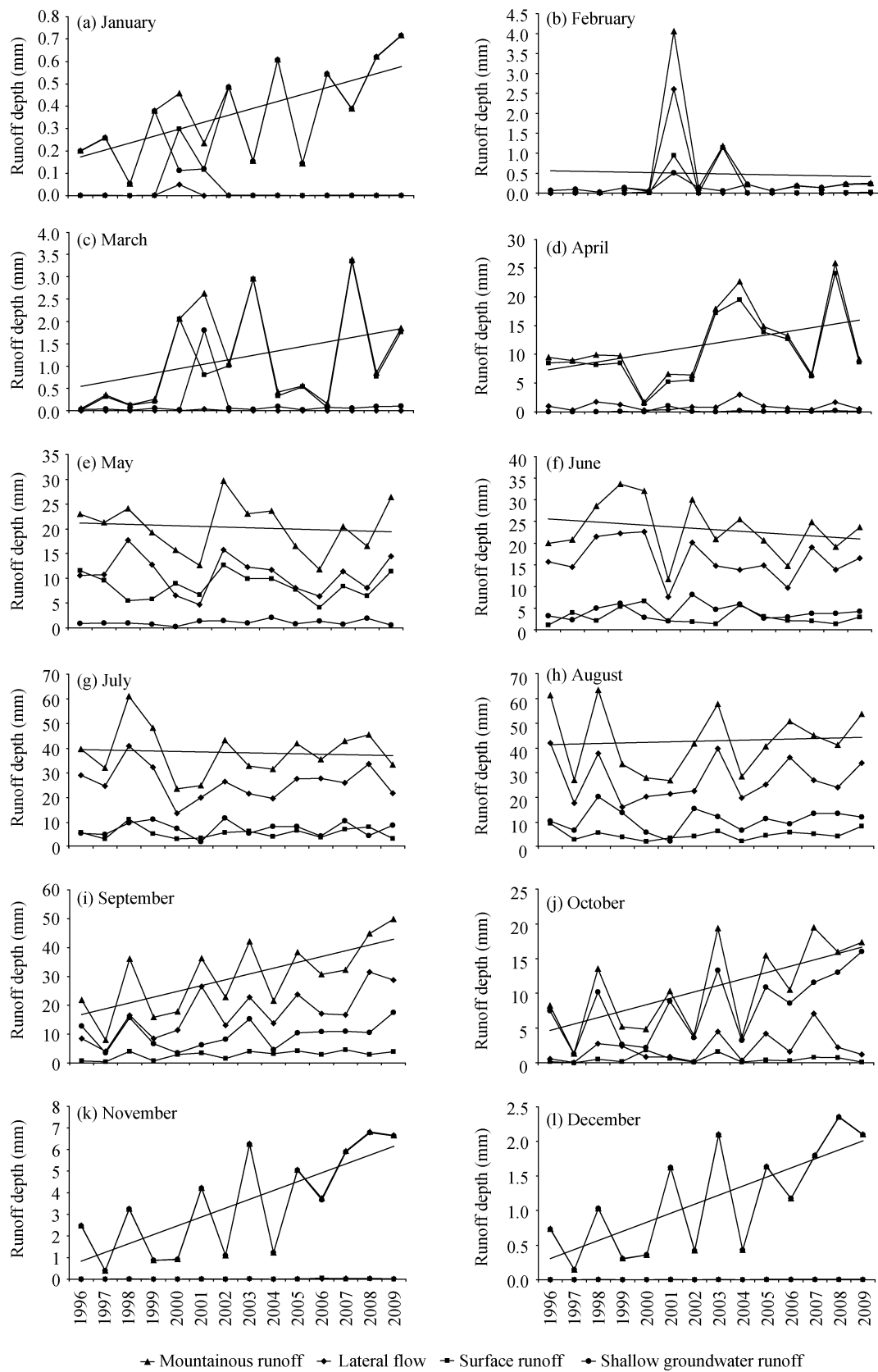
Fig. 5   Monthly variation of runoff components from 1996 to 2009

mainly by shallow groundwater from January to February and October to December, by surface runoff in March and April, and by lateral flow from May to September.

4   Conclusions

This article employed the SWAT model, a semi-distributed hydrological model, to simulate the complex hydrological processes of mountainous areas in inland river basins. We analyzed the interannual and monthly variation trends for mountainous runoff and runoff components (surface runoff, lateral flow, and shallow groundwater runoff) and elaborated the genetic mechanism underlying the variations. Three conclusions are drawn from this study.

(1) According to the precision assessment, NSE coefficients and R^2 values exceed 0.90, and PBIAS values are controlled within ±5% during the calibration and validation periods, indicating that SWAT is practicable to simulate the hydrological processes of mountainous areas in inland river basins.

(2) The multi-year monthly mean variations of the runoff components, namely surface runoff, lateral flow, and shallow groundwater runoff, reach their year-round maximums in April, July, and September, respectively. The mountainous runoff is mainly recharged by lateral flow, followed by shallow groundwater and surface runoff.

(3) The monthly variations of the mountainous runoff within a year show a slight decrease during May–July, as compared to other months. The mountainous runoff is mainly recharged by shallow groundwater in January, February, and from October to December, by surface runoff in March and April, and by lateral flow from May to September.

Acknowledgements

References

Allen R, Pereira L S, Raes D, et al. 1998. Crop evapotranspiration–Guidelines for computing crop water requirements–FAO Irrigation and drainage paper 56. Rome, Italy: United Nations FAO. http://www.fao.org/docrep/X0490E/X0490E00.htm.

Arnold J G, Srinivasan R, Williams J R. 1998. Large area hydrologic modeling and assessment. Part I: model development. Journal of the American Water Resources Association, 34: 73–89.

Chen R S, Kang E S, Zhang J S. 2002. Application of the generalized regression neural network to simulating runoff from the mountainous watersheds of inland river basins in the arid area of northwest China. Advances in Water Science, 13(1): 87–92.

Chen R S, Kang E S, Ji X B, et al. 2007. Preliminary study of the hydrological processes in the alpine meadow and permafrost regions at the headwaters of Heihe River. Journal of Glaciology and Geocryology, 29(3): 387–396.

Chen R S, Lu S H, Kang E S, et al. 2008. A distributed water-heat coupled model for mountainous watershed of an inland river basin of Northwest China (I) model structure and equations. Environmental Geology, 53(6): 1299–1309.

Cheng G D, Zhao C Y. 2008. An integrated study of ecological and hydrological processes in the inland river basin of the arid regions, China. Advances in Earth Science, 23(10): 1005–1012.

Dang S Z, Wang Z G, Liu C M. 2011. Baseflow separation and its characteristics in the upper reaches of the Heihe River Basin. Resources Science, 33(12): 2232–2237.

Fiseha B M, Setegn S G, Melesse A M, et al. 2012. Hydrological analysis of the upper Tiber River Basin, central Italy: a watershed modeling approach. Hydrological Processes, doi: 10.1002/hyp.9234.

Gao Q Z, Yang X Y. 1984. The Features of Interior Rivers and Feeding of Glacial Melt Water in the Hexi Region, Gansu Province. Beijing: Sciences Press.

Gupta H V, Sorooshian S, Yapo P O. 1999. Status of automatic calibration for hydrologic models: comparison with multilevel expert calibration. Journal of Hydrologic Engineering, 4: 135–143.

Huang Q H, Zhang W C. 2004. Improvement and application of GIS-based distributed SWAT hydrological modeling on high altitude, cold, semi-arid catchment of Heihe River Basin, China. Journal of Nanjing Forestry University: Natural Sciences Edition, 28(2): 22–26.

Huang Q H, Zhang W C. 2010. Application and parameters sensitivity analysis of SWAT model. Arid Land Geography, 33(1): 8–15.

Huang Y, Chen X, Li Y P, et al. 2012. A simulation-based two-stage interval-stochastic programming model for water resources management in Kaidu-Kongqi watershed, China. Journal of Arid Land, 4(4): 390–398.

Jia Y, Ni G, Kawahara Y, et al. 2001. Development of WEP model and its application to an urban watershed. Hydrological Processes, 15(11): 2175–2194.

Jia Y W, Wang H, Yan D H. 2006. Distributed model of hydrological cycle system in Heihe River Basin. Journal of Hydraulic Engineering, 37(5): 534–542.

Jin M, Li Y, Liu X D, et al. 2011. Interannual variation characteristics of seasonal frozen soil in upper middle reaches of Heihe River in Qilian Mountains. Journal of Glaciology and Geocryology, 33(5): 1068–1073.

Kang E S, Cheng G D, Lan Y C, et al. 1999. A model for simulating the response of runoff from the mountainous watersheds of inland river basin in the arid area of northwest China to climatic changes. Science in China: Series D, 29(Supp1.): 52–63.

Kang E S, Chen R S, Zhang Z H, et al. 2008. Some problems facing hydrological and ecological researches in the mountain watershed at the upper stream of an inland river basin. Advances in Earth Science, 23(7): 675–681.

Krause P, Boyle D, Bäse F. 2005. Advances in geosciences comparison of different efficiency criteria for hydrological model assessment. Advances in Geosciences, 5: 89–97.

Lan Y C, Kang E S, Jin H J, et al. 1999. Study on the variation characteristics and trend of mountainous runoff in the Heihe River Basin. Journal of Glaciology and Geocryology, 21(1): 49–53.

Legates D R, McCabe G J. 1999. Evaluating the use of "Goodness-of-Fit" measures in hydrologic and hydroclimatic model validation. Water Resources Research, 35(1): 233–241.

Li Z L, Xu Z X, Li Z J. 2011. Performance of WASMOD and SWAT on hydrological simulation in Yingluoxia watershed in northwest of China. Hydrological Processes, 25(13): 2001–2008.

Ling H B, Xu H L, Fu J Y, et al. 2012. Surface runoff processes and sustainable utilization of water resources in Manas River Basin, Xinjiang, China. Journal of Arid Land, 4(3): 271–280.

Moriasi D N, Arnold J G, Van Liew M W, et al. 2007. Model evaluation guidelines for systematic quantification of accuracy in watershed simulations. Transactions of The ASABE, 50: 885–900.

Morris M D. 1991. Factorial sampling plans for preliminary computational experiments. Tecnometrics, 33(2): 161–174.

Nash J, Sutcliffe J. 1970. River flow forecasting through conceptual models Part I – a discussion of principles. Journal of Hydrology, 10: 282–290.

Neitsch S L, Arnold J G, Kiniry J R, et al. 2005. Soil and Water Assessment Tool Theoretical Documentation: Version 2005. Temple, Tex.: USDA-ARS Grassland, Soil and Water Research Laboratory.

Rui X F. 1997. Some problems in research of watershed hydrology model. Advances in Water Science, 8(1): 94–98.

Stephen J B. 1986. Trends and directions in hydrology. Water Resources Research, 22(9): 1–5.

Tang Q C, Qu Y G, Zhou Y C. 1992. Water resources research of arid region in China. Beijing: Science Press, 1992.

van Griensven A, Meixner T, Grunwald S, et al. 2006. A global sensitivity analysis tool for the parameters of multi-variable catchment models. Journal of Hydrology, 324(1–4): 10–23.

Wang J, Li S. 2006. Effect of climatic change on snowmelt runoffs in mountainous regions of inland rivers in Northwestern China. Science in China: Series D, 49(8): 881–888.

Xia J, Wang G S, Lv A F, et al. 2003. A research on distributed time variant gain modeling. Acta Geographic Sinica, 58(5): 789–796.

Zhang H, Zhang B, Zhao C Y. 2011. Annual base flow change and its causes in the upper reaches of Heihe River. Geographical Research, 30(8): 1421–1430.

Zhao L J, Yin L, Xiao H L, et al. 2011. Isotopic evidence for the moisture origin and composition of surface runoff in the headwaters of the Heihe River basin. Chinese Science Bulletin, 56(4–5): 406–415.